# UC Berkeley
## UC Berkeley Previously Published Works


### Title
Franck–Condon and Herzberg–Teller Signatures in Molecular Absorption and Emission Spectra


### Permalink
https://escholarship.org/uc/item/33c9b7zs



### Journal
The Journal of Physical Chemistry B, 126(15)

### ISSN
1520-6106



### Authors
Kundu, Sohang
Roy, Partha Pratim
Fleming, Graham R
et al.



### Publication Date
2022-04-21

### DOI
10.1021/acs.jpcb.2c00846

Peer reviewed



eScholarship.org Powered by the California Digital Library
University of California

THE JOURNAL OF PHYSICAL CHEMISTRY B
A JOURNAL OF THE AMERICAN CHEMICAL SOCIETY

pubs.acs.org/JPCB

Article

# Franck–Condon and Herzberg–Teller Signatures in Molecular Absorption and Emission Spectra

Sohang Kundu, Partha Pratim Roy, Graham R. Fleming, and Nancy Makri*

Cite This: J. Phys. Chem. B 2022, 126, 2899–2911

Read Online

ACCESS | Metrics & More | Article Recommendations

**ABSTRACT:** Some molecules of chemical and biological significance possess vibrations with significant Herzberg–Teller (HT) couplings, which render the Franck–Condon (FC) approximation inadequate and cause the breakdown of the well-known mirror-image symmetry between linear absorption and emission spectra. Using a model two-state system with displaced harmonic potential surfaces, we show analytically that the FC-HT interference gives rise to asymmetric intensity modification, which has the same sign for all transitions on one side of the 0–0 absorption line and the opposite sign in the equivalent fluorescence transitions, while the trend is exactly reversed for all transitions on the other side the 0–0 line. We examine the dependence of the absorption–emission asymmetry on the mode frequency, Huang–Rhys factor, and dipole moment parameters to show the recovery of symmetry with particular combinations of parameters and a crossover from fluorescence to absorption dominance. We illustrate the analytical predictions through numerically exact calculations in models of one and two discrete vibrational modes and in the presence of a harmonic dissipative bath. In addition to homogeneous broadening effects, we identify large asymmetric shifts of absorption and emission band maxima, which can produce the illusion of unequal frequencies in the ground and excited potential surfaces as well as a nontrivial modulation of spectral asymmetry by temperature, which results from the enhancement of transitions on one side of the 0–0 line. These findings will aid the interpretation of experimental spectra in HT-active molecular systems.

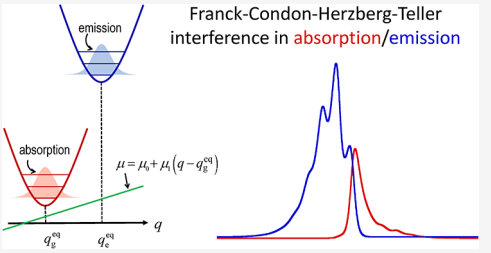


## 1. INTRODUCTION

The Franck–Condon (FC) approximation[1] offers a simple, intuitive model for understanding electronic spectra. Within the FC model, the transition moment becomes proportional to the overlap of nuclear wavefunctions on the two electronic states, whose nonmonotonic dependence on vibrational quantum numbers leads to the well-known progressions of transition intensities.[2] Perhaps surprisingly, the neglect of nuclear coordinate dependence in the electronic matrix element of the dipole moment has been shown to be adequate and sufficiently accurate for assigning spectral lines in the majority of molecular systems. However, the FC assumption is known to break down in some cases (most notably in aromatic molecules, for example in anthracene,[3] phenanthrene,[4] free-base porphyrins,[5] and metalloporphyrins[6]), and corrections become necessary for interpreting the observed transitions.[7,8] The lowest-order correction involves expanding the dipole moment matrix element $\mu$ (in the direction of the electric field) through linear terms in the normal mode coordinates

$$\mu(\mathbf{q}) \equiv \langle g|\hat{\mu}_{el-vib}|e\rangle \simeq \mu^{(0)} + \sum_k \mu_k^{(1)}(\hat{q}_k - q_k^g), \tag{1.1}$$

where $\langle g|$ and $|e\rangle$ are the ground and excited electronic states, $\mathbf{q}$ is the vector of normal mode coordinates at the equilibrium geometry $\mathbf{q}^g$ of the ground state, $\mu^{(0)}$ is the coordinate-independent component of the dipole matrix element along the field, and $\mu_k^{(1)}$ is its first derivative with respect to $q_k$. The coordinate-independent term $\mu^{(0)}$ is responsible for FC transitions, while the vector $\boldsymbol{\mu}^{(1)} = \{\mu_k^{(1)}\}$ of dipole derivatives is the Herzberg–Teller[9] (HT) coupling. Transition dipole derivatives along vibrational coordinates can arise from nonadiabatic mixing of the excited electronic state e with another state that couples to the ground state. When the g–e transition is FC-forbidden by symmetry ($\mu^{(0)} = 0$), the transition can be HT-allowed through intensity borrowing.[10] If the equilibrium geometries of the ground and excited states of interest are identical because of symmetry, the term linear in normal mode coordinates leads to $n \rightarrow n \pm 1$ transitions in this case, which can be very prominent, while higher transitions are forbidden. The electronic spectra can thus appear rather peculiar in such situations. Craig and Small have pointed out[4] that the HT term can lead to sizable corrections of the transition moments predicted by the zeroth-order FC model,

Received: February 4, 2022
Revised: March 23, 2022
Published: April 7, 2022

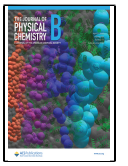

Downloaded via UNIV OF CALIFORNIA BERKELEY on April 29, 2022 at 19:35:41 (UTC).
See https://pubs.acs.org/sharingguidelines for options on how to legitimately share published articles.

ACS Publications
© 2022 American Chemical Society



https://doi.org/10.1021/acs.jpcb.2c00846
J. Phys. Chem. B 2022, 126, 2899–2911

increasing the intensity of $0 - n$ transitions in fluorescence and decreasing it in absorption. The asymmetry induced by FC-HT interference effects give rise to the breakdown of the well-known mirror-image symmetry between the absorption and emission spectra. While simulations of FC-allowed spectra are abundant in the literature, only a small fraction of computational studies (for example, see refs 4, 11−21) have included HT effects.

In this paper, we present a comprehensive study of HT effects in model molecular systems within the normal mode approximation of the relevant electronic potential energy surfaces. We show analytically and demonstrate through numerical calculations that the absorption−emission asymmetry induced by the interference between FC and HT terms has the same sign for all $m \rightarrow n$ transitions with $m > n$ and the opposite sign for $m < n$. When the two dipole parameters ($\mu^{(0)}$and $\mu_k^{(1)}$) have the same sign, emission intensity is enhanced for all transitions that lie on the red side of the 0−0 line in the fluorescence spectrum relative to the corresponding lines on the blue side of the 0−0 line in absorption, while all intensities on the blue side of the 0−0 emission line are diminished compared to their absorption counterparts. These trends are reversed when the dipole moment parameters have opposite signs. Our analysis suggests that this asymmetry depends nonmonotonically on the dipole moment components and the Huang−Rhys factor of a mode, and reverses signs as these parameters are varied, going through a narrow region of parameter space where the mirror-image symmetry is recovered. Depending on the ground−excited potential geometry and the dipole parameters, these effects can be similar or opposite for each normal mode vibration, giving rise to combination bands that exhibit rich patterns in the spectra as well as interesting temperature effects.

When the electronic states are also coupled to an FC-active solvent or matrix, homogeneous broadening can blur and merge vibrational lines. The majority of earlier studies have treated such effects by using Gaussian or Lorentzian functions to broaden the computed spectral lines. In this paper, we account for the dynamical process responsible for homogeneous broadening by including a harmonic dissipative bath that mimics a condensed-phase environment. We show that the absorption−emission asymmetry can lead to large shifts of band maxima, giving the erroneous impression of unequal ground and excited potential energy curvatures. Since the interference-induced enhancement of the spectral lines flips sign as one moves from the red to the blue side of the 0−0 transition, the spectra become asymmetrically broadened. These effects are accompanied by a nontrivial temperature dependence, as the thermal population of higher vibrational states generates spectral lines and bands preferentially on one of the two sides of the $n-n$ line.

In Section 2, we set up the two-state Hamiltonian in the normal mode approximation and the expansion of the dipole moment. We also give the expressions for the time correlation functions that we use to calculate thermally averaged spectra with several discrete modes and a dissipative harmonic bath. In Section 3, we derive the contributions of the FC and HT terms and the relevant line intensities. We show that the asymmetry of a transition (i.e., the difference of the absorption and emission intensities) is of the same type for all $m \rightarrow n$ transitions on the same (red or blue) side of the 0−0 line but switches signs on the other side, and that it has opposite signs in absorption and fluorescence. Using an analytical expression, we show the quantitative dependence of the spectral asymmetry as a function of mode frequency, the Huang−Rhys factor, and dipole terms. In Section 4, we illustrate these results by showing the spectra that result with several model parameters in the case of a single vibrational mode and with two vibrations, which give rise to combination bands. The effects of condensed-phase environments are investigated in Section 5, where we show spectra with one or two discrete vibrational modes in the presence of a harmonic dissipative bath. Last, we conclude in Section 6 with a summary of our findings and some additional remarks.

## 2. BACKGROUND

In this section, we introduce a model Hamiltonian, discuss the relevant observables, such as the spectral lineshapes, and motivate initial conditions based on experimental approaches. We illustrate the required expressions and outline a dynamical approach to compute finite-temperature absorption and emission spectra under the FC and HT approximations.

**2.1. Model Hamiltonian.** Consider a molecule, with ground and excited electronic states $|g\rangle$ and $|e\rangle$, respectively, characterized by the parameters $s_g$ and $s_e$ (which have dimensions of length). We assume that the vibrational and solvent coordinates can be described as a set of harmonic modes with frequencies $\omega_k$, whose coupling to the electronic states is characterized by the parameters $c_k$. The total Hamiltonian is given by

$$\hat{H}_{\mathrm{el-vib}} = (\varepsilon_g + \hat{H}_g)|g\rangle\langle g| + (\varepsilon_e + \hat{H}_e)|e\rangle\langle e| \tag{2.1}$$

$$\hat{H}_g = \sum_k \frac{\hat{p}_k^2}{2m} + \frac{1}{2}m\omega_k^2(\hat{q}_k - q_{g,k}^{eq})^2,$$

$$\hat{H}_e = \sum_k \frac{\hat{p}_k^2}{2m} + \frac{1}{2}m\omega_k^2(\hat{q}_k - q_{e,k}^{eq})^2 \tag{2.2}$$

where $q_k$ and $p_k$ are the coordinates and momenta of the harmonic modes, $\varepsilon_g$ and $\varepsilon_e$ are the energies of the ground and excited states, and $q_{g,k}^{eq}$ and $q_{e,k}^{eq}$ denote the normal mode coordinates of the two potential surfaces at their equilibrium geometries, which are given by $q_{g,k}^{eq} = c_k s_g/m\omega_k^2$ and $q_{e,k}^{eq} = c_k s_e/m\omega_k^2$. The coupling of molecular modes to the electronic states is often specified in terms of the Huang−Rhys factors, $S_k$, which are given by

$$S_k = \frac{c_k^2}{2\hbar m\omega_k^3}\Delta s^2 \tag{2.3}$$

where $\Delta s = s_e - s_g$. The arrangement of the potential surfaces is shown in Figure 1. We note that eq 2.2 assumes that the normal mode parameters on the two potential surfaces are identical. Even though Duschinsky effects[22] have been found to play an important role in connection with HT contributions to the molecular spectra,[11] the main effect in this regard is a modification of the terms that contribute to FC-HT interference. The neglect of Duschinsky rotation in the present study allows an all-analytical examination of FC-HT interference effects, which lead to simple results and important insights about spectral trends.

**2.2. Lineshapes and Initial Condition.** We calculate the absorption and emission spectral lineshapes, $\sigma_A(\omega)$ and $\sigma_E(\omega)$, respectively, as the real parts of the following Fourier transforms[23,24]



https://doi.org/10.1021/acs.jpcb.2c00846
J. Phys. Chem. B 2022, 126, 2899−2911

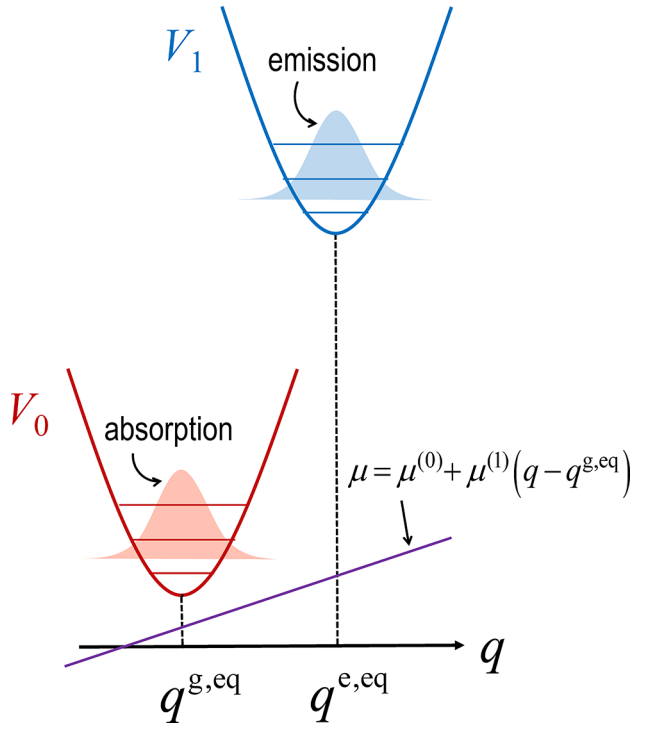


**Figure 1.** A schematic showing the two potential energy surfaces along a vibrational coordinate $q$ and the initially equilibrated densities for absorption and emission spectra. The linearized dipole moment function is also shown.

$$\sigma_A(\omega) \propto \mathrm{Re}\int_0^\infty e^{i\omega t} R_A(t)\, dt \quad \text{and}$$
$$\sigma_E(\omega) \propto \mathrm{Re}\int_0^\infty e^{-i\omega t} R_E(t) dt \tag{2.4}$$

Here, $R_A(t)$ and $R_E(t)$ are the corresponding dipole−dipole autocorrelation functions given by[25]

$$R_A(t) = \mathrm{Tr}[\hat{\mu}_{el-vib}\, e^{-i\hat{H}t/\hbar}\hat{\mu}_{el-vib}\,\hat{\rho}_A(0)\, e^{i\hat{H}t/\hbar}],\ R_E(t) = \mathrm{Tr}[\hat{\mu}_{el-vib} e^{-i\hat{H}t/\hbar}\hat{\mu}_{el-vib}\,\hat{\rho}_E(0)\, e^{i\hat{H}t/\hbar}] \tag{2.5}$$

$\hat{\mu}_{el\text{-}vib}$ is the transition dipole operator in the direction of the electric field, and the initial density matrices for absorption and emission are denoted by $\hat{\rho}_A(0)$ and $\hat{\rho}_E(0)$, respectively.

In the absorption experiment, the molecule is initially in thermal equilibrium with its surroundings on the ground electronic state before optical excitation; thus,

$$\hat{\rho}_A(0) = |g\rangle\langle g| Z^{-1} e^{-\beta\hat{H}_g} \tag{2.6}$$

where $Z$ is the partition function of the vibrational bath. In contrast, spontaneous emission de-excites the molecule, which, in the condensed phase, has generally fully relaxed within the excited state prior to significant emission, i.e.,

$$\hat{\rho}_E(0) = |e\rangle\langle e| Z^{-1} e^{-\beta\hat{H}_e} \tag{2.7}$$

Next, we note that for transitions between the two chosen states, the projection of the dipole operator along the direction of the electric field can be expressed in the form

$$\hat{\mu}_{el-vib} = (|g\rangle\langle e| + |e\rangle\langle g|)\hat{\mu} \tag{2.8}$$

where $\hat{\mu}$ is the vibrational/solvent component that generally depends on the bath coordinates.

Using the last two equations and taking advantage of the diagonal form of the Hamiltonian in eq 2.1, the dipole autocorrelation functions can be easily simplified to

$$R_A(t) = e^{-i(\varepsilon_e-\varepsilon_g)t/\hbar}\, Z^{-1}\, \mathrm{Tr}(\hat{\mu} e^{-i\hat{H}_e t/\hbar}\hat{\mu} e^{-\beta\hat{H}_g} e^{i\hat{H}_g t/\hbar}),$$
$$R_E(t) = e^{i(\varepsilon_e-\varepsilon_g)t/\hbar}\, Z^{-1}\, \mathrm{Tr}(\hat{\mu} e^{-i\hat{H}_g t/\hbar}\hat{\mu} e^{-\beta\hat{H}_e} e^{i\hat{H}_e t/\hbar}) \tag{2.9}$$

where the trace is with respect to the vibrational and solvent degrees of freedom.

**2.3. Franck−Condon and Herzberg−Teller Approximations.** We now expand the dipole moment operator $\hat{\mu}$ in a Taylor series along all vibrational modes $\mathbf{q} = \{q_k\}$ around the coordinates of the ground state potential minimum $\mathbf{q}_g^{eq}$. Within the HT approximation,

$$\mu(\mathbf{q}) \simeq \mu^{(0)} + \sum_k \mu_k^{(1)}(\hat{q}_k - q_{g,k}^{eq}) \tag{2.10}$$

where

$$\mu^{(0)} = \mu\,|_{\mathbf{q}=\mathbf{q}_g^{eq}} \tag{2.11}$$

is the component responsible for FC transitions and

$$\mu_k^{(1)} = \left(\frac{\partial\mu}{\partial q_k}\right)_{\mathbf{q}=\mathbf{q}_g^{eq}} \tag{2.12}$$

are the HT coupling coefficients.

The Franck−Condon (FC) approximation, which corresponds to a "vertical" excitation or de-excitation of the electronic-vibrational density from one potential surface to another while the nuclear coordinates are frozen, is obtained by truncating the expansion of the dipole moment at the zeroth-order term, $\mu(\mathbf{q}) \simeq \mu^{(0)}$, and leads to the following expressions for the dipole autocorrelation functions:

$$R_A^{FC}(t) = e^{-i(\varepsilon_e-\varepsilon_g)t/\hbar}|\mu^{(0)}|^2\, Z^{-1}\, \mathrm{Tr}(e^{-i\hat{H}_e t/\hbar} e^{-\beta\hat{H}_g} e^{i\hat{H}_g t/\hbar})$$
$$R_E^{FC}(t) = e^{i(\varepsilon_e-\varepsilon_g)t/\hbar}|\mu^{(0)}|^2\, Z^{-1}\, \mathrm{Tr}(e^{-i\hat{H}_g t/\hbar} e^{-\beta\hat{H}_e} e^{i\hat{H}_e t/\hbar}) \tag{2.13}$$

The full FC-HT correlation functions (for either absorption or emission) can be decomposed into FC, HT, and FC-HT (interference) contributions,

$$R(t) = R^{FC}(t) + R^{HT}(t) + R^{FC-HT}(t) \tag{2.14}$$

where the HT term arises purely from HT couplings. This term is given by the expressions

$$R_A^{HT}(t) = e^{-i(\varepsilon_e-\varepsilon_g)t/\hbar}\sum_k \mu_k^{(1)}\sum_{k'}\mu_{k'}^{(1)}\, Z^{-1}\, \mathrm{Tr}[(\hat{q}_k - q_{g,k}^{eq}) e^{-i\hat{H}_e t/\hbar}(\hat{q}_{k'} - q_{g,k'}^{eq}) e^{-\beta\hat{H}_g} e^{i\hat{H}_g t/\hbar}]$$
$$R_E^{HT}(t) = e^{i(\varepsilon_e-\varepsilon_g)t/\hbar}\sum_k \mu_k^{(1)}\sum_{k'}\mu_{k'}^{(1)}\, Z^{-1}\, \mathrm{Tr}[(\hat{q}_k - q_{g,k}^{eq}) e^{-i\hat{H}_g t/\hbar}(\hat{q}_{k'} - q_{g,k'}^{eq}) e^{-\beta\hat{H}_e} e^{i\hat{H}_e t/\hbar}] \tag{2.15}$$

The FC-HT interference terms for absorption and emission are given by



https://doi.org/10.1021/acs.jpcb.2c00846
J. Phys. Chem. B 2022, 126, 2899−2911

$$
\begin{aligned}
R_{\mathrm{A}}^{\mathrm{FC-HT}}(t) &= \mathrm{e}^{-i(\varepsilon_{\mathrm{e}}-\varepsilon_{\mathrm{g}})t/\hbar}\mu^{(0)}\sum_k \mu_k^{(1)} Z^{-1}\mathrm{Tr}[\mathrm{e}^{-i\hat{H}_{\mathrm{e}}t/\hbar}(\hat{q}_k - q_{\mathrm{g},k}^{\mathrm{eq}})\mathrm{e}^{-\beta\hat{H}_{\mathrm{g}}}\mathrm{e}^{i\hat{H}_{\mathrm{g}}t/\hbar}] \\
&+ \mathrm{e}^{-i(\varepsilon_{\mathrm{e}}-\varepsilon_{\mathrm{g}})t/\hbar}\mu^{(0)}\sum_k \mu_k^{(1)} Z^{-1}\mathrm{Tr}[(\hat{q}_k - q_{\mathrm{g},k}^{\mathrm{eq}})\mathrm{e}^{-i\hat{H}_{\mathrm{e}}t/\hbar}\mathrm{e}^{-\beta\hat{H}_{\mathrm{g}}}\mathrm{e}^{i\hat{H}_{\mathrm{g}}t/\hbar}] \\
R_{\mathrm{E}}^{\mathrm{FC-HT}}(t) &= \mathrm{e}^{i(\varepsilon_{\mathrm{e}}-\varepsilon_{\mathrm{g}})t/\hbar}\mu^{(0)}\sum_k \mu_k^{(1)} Z^{-1}\mathrm{Tr}[\mathrm{e}^{-i\hat{H}_{\mathrm{g}}t/\hbar}(\hat{q}_k - q_{\mathrm{g},k}^{\mathrm{eq}})\mathrm{e}^{-\beta\hat{H}_{\mathrm{e}}}\mathrm{e}^{i\hat{H}_{\mathrm{e}}t/\hbar}] \\
&+ \mathrm{e}^{i(\varepsilon_{\mathrm{e}}-\varepsilon_{\mathrm{g}})t/\hbar}\mu^{(0)}\sum_k \mu_k^{(1)} Z^{-1}\mathrm{Tr}[(\hat{q}_k - q_{\mathrm{g},k}^{\mathrm{eq}})\mathrm{e}^{-i\hat{H}_{\mathrm{g}}t/\hbar}\mathrm{e}^{-\beta\hat{H}_{\mathrm{e}}}\mathrm{e}^{i\hat{H}_{\mathrm{e}}t/\hbar}]
\end{aligned}
\tag{2.16}
$$

Many approaches are available for evaluating these correlation functions. A simple procedure is obtained from the quantum-classical path integral (QCPI) formulation,[26−28] which is derived by using Feynman's path integral[29,30] representation in the semiclassical limit with respect to the coordinates of the nuclei. The QCPI expression is designed for use with anharmonic potential surfaces where the dynamical effects are efficiently captured through classical trajectories subject to forces along quantum paths of the electronic system. In the case of harmonic potentials, the QCPI methodology is exact. In the present case of eqs 2.13−2.16, the forces supplied by the forward and backward evolution operators are constant, allowing single-step evaluation. Further, the correlation functions can be further decomposed into products of one-dimensional Gaussian integrals that can be evaluated analytically. Finally, Fourier transformation of the correlation functions gives the absorption and emission lineshapes. The procedure is described in Appendix A.

## 3. FRANCK−CONDON AND HERZBERG−TELLER INTERFERENCE AND ABSORPTION−EMISSION ASYMMETRY

By adjusting the zeroth order term $\mu^{(0)}$, it is useful to recast eq 2.10 in the form

$$
\mu(\mathbf{q}) \simeq \tilde{\mu}^{(0)} + \sum_k \mu_k^{(1)}(\hat{q}_k - q_{\mathrm{M},k}^{\mathrm{eq}}) \tag{3.1}
$$

where

$$
\begin{aligned}
\tilde{\mu}^{(0)} &= \mu^{(0)} + \frac{1}{2}\sum_k \mu_k^{(1)}(q_{\mathrm{e},k}^{\mathrm{eq}} - q_{\mathrm{g},k}^{\mathrm{eq}}),\ q_{\mathrm{M},k}^{\mathrm{eq}} \\
&= \frac{1}{2}(q_{\mathrm{g},k}^{\mathrm{eq}} + q_{\mathrm{e},k}^{\mathrm{eq}})
\end{aligned}
\tag{3.2}
$$

Equation 3.1 expresses the dipole moment with respect to the midpoint between the equilibrium geometries of the ground and excited surfaces. If the coordinate-independent term $\tilde{\mu}^{(0)}$ is equal to zero, eq 3.1 is a line passing through the midpoint $\mathbf{q}_{\mathrm{M}}^{\mathrm{eq}}$ of the two potential minima. As will be shown below, this symmetric situation leads to absorption and emission spectra that form a mirror-image pair analogous to the situation observed in the absence of HT terms.

In the rest of this section, we consider a single vibrational degree of freedom and (for clarity) drop the mode subscript $k$. Consider a transition between vibrational state $m$ in the ground potential and state $n$ of the excited potential. We define the FC and HT matrix elements between the two vibrational states $\Phi_m^{\mathrm{g}}$, $\Phi_n^{\mathrm{e}}$

$$
\begin{aligned}
f_{mn} &\equiv \langle\Phi_m^{\mathrm{g}}|\Phi_n^{\mathrm{e}}\rangle = \int_{-\infty}^{\infty}\phi_m(q - q_{\mathrm{g}}^{\mathrm{eq}})\phi_n(q - q_{\mathrm{e}}^{\mathrm{eq}})\,\mathrm{d}q \\
h_{mn} &\equiv \langle\Phi_m^{\mathrm{g}}|\hat{q} - q_{\mathrm{M}}^{\mathrm{eq}}|\Phi_n^{\mathrm{e}}\rangle \\
&= \int_{-\infty}^{\infty}\phi_m(q - q_{\mathrm{g}}^{\mathrm{eq}})(\hat{q} - q_{\mathrm{e}}^{\mathrm{eq}})\phi_n(q - q_{\mathrm{e}}^{\mathrm{eq}})\,\mathrm{d}q
\end{aligned}
\tag{3.3}
$$

where $\phi_i$ are harmonic oscillator wavefunctions. The FC integral can be rewritten in the more symmetric form

$$
\begin{aligned}
f_{mn} &= \int_{-\infty}^{\infty}\phi_m\left(q - q_{\mathrm{M}}^{\mathrm{eq}} + \frac{1}{2}\Delta q_{\mathrm{ge}}^{\mathrm{eq}}\right)\phi_n\left(q - q_{\mathrm{M}}^{\mathrm{eq}} - \frac{1}{2}\Delta q_{\mathrm{ge}}^{\mathrm{eq}}\right)\mathrm{d}q \\
&= \int_{-\infty}^{\infty}\phi_m\left(x + \frac{1}{2}\Delta q_{\mathrm{ge}}^{\mathrm{eq}}\right)\phi_n\left(x - \frac{1}{2}\Delta q_{\mathrm{ge}}^{\mathrm{eq}}\right)\mathrm{d}x
\end{aligned}
\tag{3.4}
$$

where $\Delta q_{\mathrm{ge}}^{\mathrm{eq}} = q_{\mathrm{e}}^{\mathrm{eq}} - q_{\mathrm{g}}^{\mathrm{eq}}$. Substituting $x \to -x$, it is easy to show that if both $\phi_m$ and $\phi_n$ are even, or if both are odd functions of their coordinates (i.e., both $m$,$n$ are either even or odd),

$$
\begin{aligned}
f_{mn} &= \int_{-\infty}^{\infty}\phi_m\left(-x + \frac{1}{2}\Delta q_{\mathrm{ge}}^{\mathrm{eq}}\right)\phi_n\left(-x - \frac{1}{2}\Delta q_{\mathrm{ge}}^{\mathrm{eq}}\right)\mathrm{d}x \\
&= \int_{-\infty}^{\infty}\phi_n\left(x + \frac{1}{2}\Delta q_{\mathrm{ge}}^{\mathrm{eq}}\right)\phi_m\left(x - \frac{1}{2}\Delta q_{\mathrm{ge}}^{\mathrm{eq}}\right)\mathrm{d}x = \langle\Phi_n^{\mathrm{g}}|\Phi_m^{\mathrm{e}}\rangle = f_{nm}
\end{aligned}
\tag{3.5}
$$

whereas if one of these wavefunctions is even and the other is odd,

$$
f_{mn} = -\int_{-\infty}^{\infty}\phi_m\left(x - \frac{1}{2}\Delta q_{\mathrm{ge}}^{\mathrm{eq}}\right)\phi_n\left(x + \frac{1}{2}\Delta q_{\mathrm{ge}}^{\mathrm{eq}}\right)\mathrm{d}x = -f_{nm} \tag{3.6}
$$

Similarly, it is straightforward to show that if both $m$ and $n$ (i.e., if $\phi_m$ and $\phi_n$) are even, or if both are odd, then

$$
h_{mn} = -\langle\Phi_n^{\mathrm{g}}|\hat{q} - q_{\mathrm{M}}^{\mathrm{eq}}|\Phi_m^{\mathrm{e}}\rangle = -h_{nm} \tag{3.7}
$$

while

$$
h_{mn} = h_{nm} \tag{3.8}
$$

if one of these functions is even and the other is odd. In the special case $m = 0$, $n = 1$, eqs 3.6 and 3.8 agree with the observations reported in earlier work,[4,12] although according to eqs 3.5 and 3.7, the generalization to all $n$ values[12] was incorrect. We now examine the consequences of the relation between the FC and HT integrals for absorption and emission intensities.

The dipole moment matrix element for absorption between vibrational state $m$ on the ground surface and state $n$ on the excited surface is given by

$$
\mu_{m\to n}^{\mathrm{A}} \equiv \langle\Phi_m^{\mathrm{g}}|\hat{\mu}|\Phi_n^{\mathrm{e}}\rangle = \tilde{\mu}^{(0)}f_{mn} + \mu^{(1)}h_{mn} \tag{3.9}
$$

Using the results obtained above, the matrix element for emission between the vibrational state $m$ on the excited potential and state $n$ on the ground state is

$$
\begin{aligned}
\mu_{n\leftarrow m}^{\mathrm{E}} &\equiv \langle\Phi_n^{\mathrm{g}}|\hat{\mu}|\Phi_m^{\mathrm{e}}\rangle = \tilde{\mu}^{(0)}f_{nm} + \mu^{(1)}h_{nm} \\
&= \pm(\tilde{\mu}^{(0)}f_{mn} - \mu^{(1)}h_{mn})
\end{aligned}
\tag{3.10}
$$

where the overall sign depends on whether the two vibrational wavefunctions have the same parity. Equations 3.9 and 3.10 are analogous to expressions reported by Craig and Small[4] for $0 \to n$ transitions. Adding and subtracting, we obtain


https://doi.org/10.1021/acs.jpcb.2c00846
J. Phys. Chem. B 2022, 126, 2899−2911

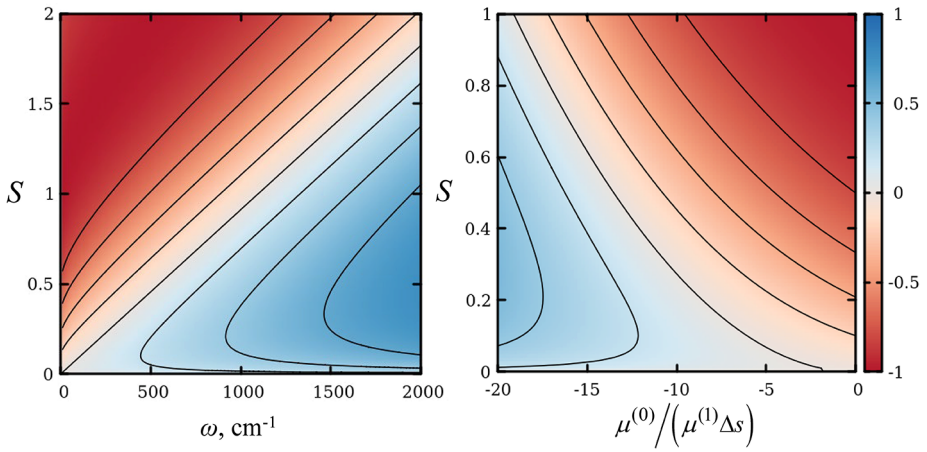


**Figure 2.** The asymmetry function $\zeta_{01}$, eq 3.19. Left: as a function of the Huang–Rhys factor and mode frequency for $\mu^{(1)}\Delta s/\mu^{(0)} = -0.1$. Right: as a function of the Huang–Rhys factor and the ratio of dipole moment terms for $\omega = 300$ cm$^{-1}$.

$$\mu^{A}_{m\to n} + \mu^{E}_{n\leftarrow m} = 2\tilde{\mu}^{(0)} f_{mn}, \quad \mu^{A}_{m\to n} - \mu^{E}_{n\leftarrow m} = 2\mu^{(1)} h_{mn} \tag{3.11}$$

if both quantum numbers are even or both are odd, or

$$\mu^{A}_{m\to n} + \mu^{E}_{n\leftarrow m} = 2\mu^{(1)} h_{mn}, \quad \mu^{A}_{m\to n} - \mu^{E}_{n\leftarrow m} = 2\tilde{\mu}^{(0)} f_{mn} \tag{3.12}$$

if only one is even. These relations can be useful for extracting Huang–Rhys factors and dipole moment parameters from experimental spectra.

Further, eqs 3.9 and 3.10 give

$$|\mu^{A}_{m\to n}|^2 = (\tilde{\mu}^{(0)} f_{mn} + \mu^{(1)} h_{mn})^2,$$
$$|\mu^{E}_{n\leftarrow m}|^2 = (\tilde{\mu}^{(0)} f_{mn} - \mu^{(1)} h_{mn})^2 \tag{3.13}$$

Depending on the signs of the dipole moment components, HR factors, and coordinate matrix elements, the two terms in the absorption and emission intensities will interfere either constructively or destructively. Thus, for a given $m,n$ pair, if the FC and HT terms interfere constructively in the intensity of an absorption line, they will interfere destructively in the emission intensity, and vice versa.[4] In the absence of HT effects, absorption and emission intensities are equal, giving rise to the well-known mirror-image symmetry. The HT contribution lowers the intensity in one of the spectra while increasing it in the other.

Equation 3.13 also shows that mirror-symmetric spectra arise if either $\mu^{(1)} = 0$ or $\tilde{\mu}^{(0)} = 0$. The first case is the well-known situation of pure FC spectra. The second case is observed if

$$\mu^{(0)} + \frac{1}{2}\sum_k \mu_k^{(1)}(q_k^{e} - q_k^{g}) = 0. \tag{3.14}$$

As discussed in the previous section, the dipole moment is usually expanded with respect to the equilibrium geometry of the ground electronic state. Equation 3.14 shows that the absorption–emission mirror-image symmetry is broken through FC-HT interference, even if $\mu^{(0)} = 0$.

To determine the direction of absorption–emission asymmetry, we examine the signs of the FC and HT integrals. While wavefunction signs are arbitrary, we adopt the convention $f_{mn} > 0$ if both quantum numbers are either even or odd, and $f_{mn} < 0$ if only one of the two quantum numbers is even and $m < n$ ($f_{mn} > 0$ for $m > n$). These signs are observed with the common convention of Hermite polynomials for small Huang–Rhys factors. Using the midpoint-shifted variables, the HT matrix element can be decomposed into two terms,

$$h_{mn} = \int_{-\infty}^{\infty} \phi_m\left(x + \frac{1}{2}\Delta q_{ge}^{eq}\right)\left(x + \frac{1}{2}\Delta q_{ge}^{eq}\right)\phi_n\left(x - \frac{1}{2}\Delta q_{ge}^{eq}\right) dx - \frac{1}{2}\Delta q_{ge}^{eq} f_{mn} \tag{3.15}$$

Expressing $x + \frac{1}{2}\Delta q_{ge}^{eq}$ in terms of raising and lowering operators, eq 3.15 becomes

$$h_{mn} = \sqrt{\frac{\hbar}{2\omega}}(\sqrt{m} f_{m-1,n} + \sqrt{m+1} f_{m+1,n}) - \frac{1}{2}\Delta q_{ge}^{eq} f_{mn} \tag{3.16}$$

(where we have set the mass equal to 1 in order to avoid confusion). If both quantum numbers are either even or odd and $m < n$, it is easy to see that $h_{nm} < 0$. On the other hand, if only one of the two quantum numbers is even, eq 3.16 leads to $h_{nm} > 0$ for $m < n$.

Gathering these results, we find that for $m < n$, the signs of $f_{mn}$ and $h_{mn}$ are opposite. Using again the relations established at the beginning of this section, we conclude that both $f_{mn}$ and $h_{mn}$ are positive for $m > n$. Thus, for lines to the right of the 0–0 absorption peak ($\hbar\omega > \varepsilon_e - \varepsilon_g$) or to the left of the 0–0 emission peak ($\hbar\omega < \varepsilon_e - \varepsilon_g$), we find that

$$|\mu^{A}_{m\to n}|^2 = (\tilde{\mu}^{(0)}|f_{mn}| - \mu^{(1)}|h_{mn}|)^2$$
$$|\mu^{E}_{n\leftarrow m}|^2 = (\tilde{\mu}^{(0)}|f_{mn}| + \mu^{(1)}|h_{mn}|)^2 \quad \text{for } m < n \tag{3.17}$$

If $\tilde{\mu}^{(0)}$ and $\mu^{(1)}$ are positive, emission is enhanced while absorption is diminished. The opposite scenario applies to lines to the left of the 0–0 absorption peak ($\hbar\omega < \varepsilon_e - \varepsilon_g$) and to the right of the 0–0 emission peak ($\hbar\omega > \varepsilon_e - \varepsilon_g$).

$$|\mu^{A}_{m\to n}|^2 = (\tilde{\mu}^{(0)}|f_{mn}| + \mu^{(1)}|h_{mn}|)^2$$
$$|\mu^{E}_{n\leftarrow m}|^2 = (\tilde{\mu}^{(0)}|f_{mn}| - \mu^{(1)}|h_{mn}|)^2 \quad \text{for } m > n \tag{3.18}$$

From eq 3.13, we see that the asymmetry of the line, i.e., the difference of the absorption and emission intensities divided by their sum, is given by



https://doi.org/10.1021/acs.jpcb.2c00846
J. Phys. Chem. B 2022, 126, 2899–2911

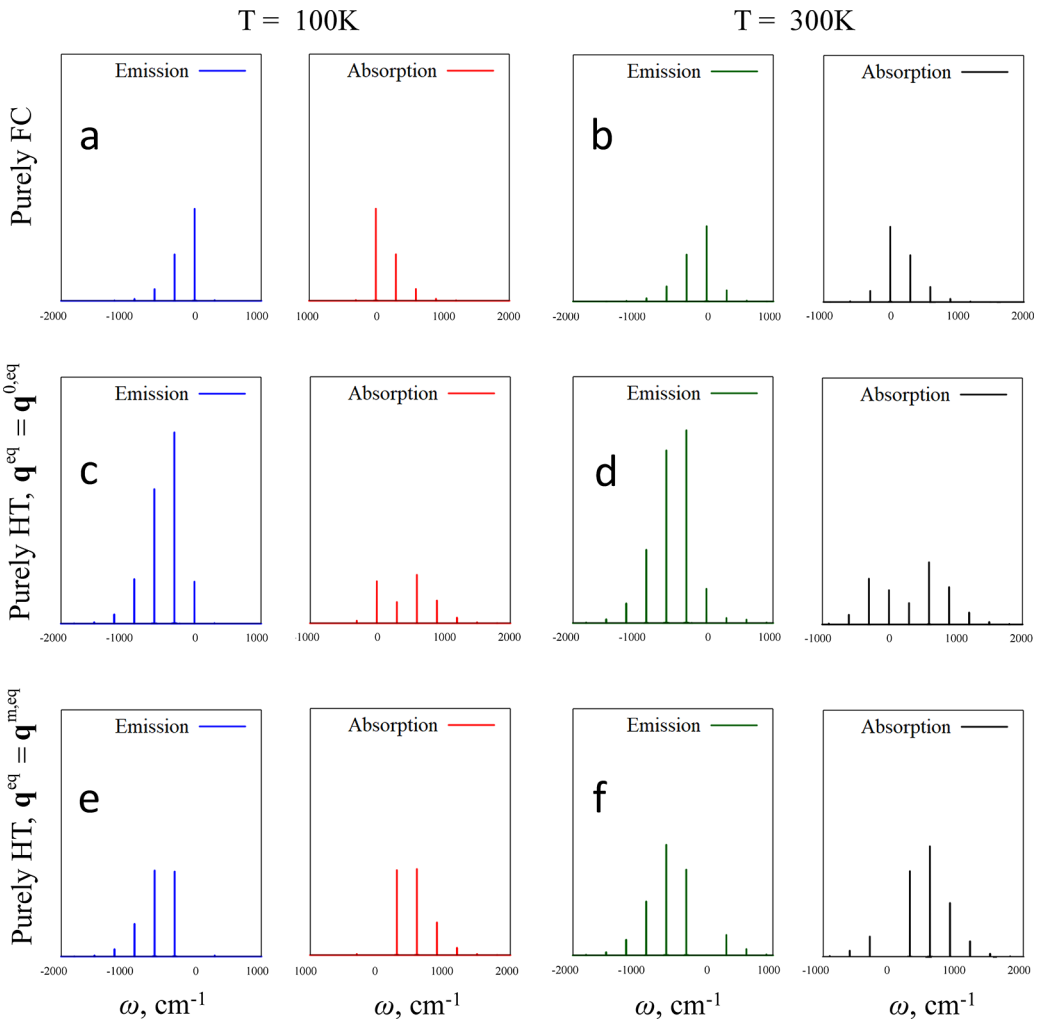


**Figure 3.** Absorption and emission spectra for a molecule with a single vibrational mode of frequency $\omega_1$ = 300 cm$^{-1}$. The frequency axes have been shifted by $(\varepsilon_e - \varepsilon_g)/\hbar$. (a, b) Pure FC spectra ($\mu_1^{(1)} = 0$) with $S_1 = 0.5$. (c, d) Pure HT spectra with $\mu^{(0)} = 0$, $S_1 = 0.5$. (e, f) FC-HT spectra with $\tilde{\mu}^{(0)} = 0$. Left: $T$ = 100 K. Right: $T$ = 300 K.

$$\zeta_{mn} \equiv \frac{|\mu^{A}_{m\to n}|^2 - |\mu^{E}_{m\to n}|^2}{|\mu^{A}_{m\to n}|^2 + |\mu^{E}_{m\to n}|^2} = \frac{2\tilde{\mu}^{(0)}\mu^{(1)} f_{mn} h_{mn}}{(\tilde{\mu}^{(0)} f_{mn})^2 + (\mu^{(1)} h_{mn})^2} \tag{3.19}$$

which, as expected, vanishes if either $\tilde{\mu}^{(0)}$ or $\mu^{(1)}$ is equal to zero.

Equations 3.17−3.19 are the main results of this section. Several noteworthy remarks can be made based on these expressions. First, we note that in the special case $S = 0$, the ground state and midpoint expansions coincide; thus, $\tilde{\mu}^{(0)} = \mu^{(0)}$. Since the two potential surfaces are undisplaced in this case, the FC and HT integrals are nonzero only for select combinations of quantum numbers. Specifically, the FC factor becomes $f_{nm} = \delta_{nm}$ (which describes FC-allowed $n-n$ transitions), while the HT matrix element is $h_{mn} = \sqrt{\hbar}\,(\sqrt{m}\,\delta_{m-1,n} + \sqrt{n}\,\delta_{m+1,n})/\sqrt{2\omega}$ (which corresponds to HT-allowed $\Delta n = \pm 1$ transitions). Since at least one of the $f_{mn}$ and $h_{mn}$ vanishes for any choice of quantum numbers in this case, we conclude from eq 3.19 that $\zeta_{mn} = 0$ for all lines, i.e., mirror-image symmetry is restored in full FC-HT spectra if the Huang−Rhys factor is equal to zero. Figure 2 shows the asymmetry function $\zeta_{01}$ as a function of the dipole moment parameters, mode frequency, and Huang−Rhys factor. In the regions where this function is positive, the absorption line has higher intensity compared to the analogous emission line, and vice versa.

Next, the midpoint-shifted constant term $\tilde{\mu}^{(0)}$ depends on the displacement between the ground and excited potential surfaces, i.e., on the Huang−Rhys factor.

$$\tilde{\mu}^{(0)} = \mu^{(0)} + \frac{1}{2}\frac{\mu^{(1)}}{m}\sqrt{\frac{2S}{\omega}} \tag{3.20}$$

Since the $S$ dependence is only in one of the two terms, the Huang−Rhys factor can change the contribution of the FC term and thus modulate the asymmetry between absorption and emission intensities. If $\mu^{(0)}\mu^{(1)} > 0$ (i.e., if both parameters are either positive or negative), increase of the Huang−Rhys factor will increase $|\tilde{\mu}^{(0)}|$ and thus further amplify the intensity of (absorption or fluorescence) transitions in the region (to the left or the right of the 0−0 line) where constructive interference is observed. In contrast, if $\mu^{(0)}\mu^{(1)} < 0$, eq 3.20 goes through zero at a critical value $S_c$ of the Huang−Rhys factor, for which absorption and emission spectra exhibit mirror-image symmetry. In this case, the spectral asymmetry is reversed as $S$ goes through this critical value. This implies that the absorption and emission spectra of two modes with


https://doi.org/10.1021/acs.jpcb.2c00846
J. Phys. Chem. B 2022, 126, 2899−2911

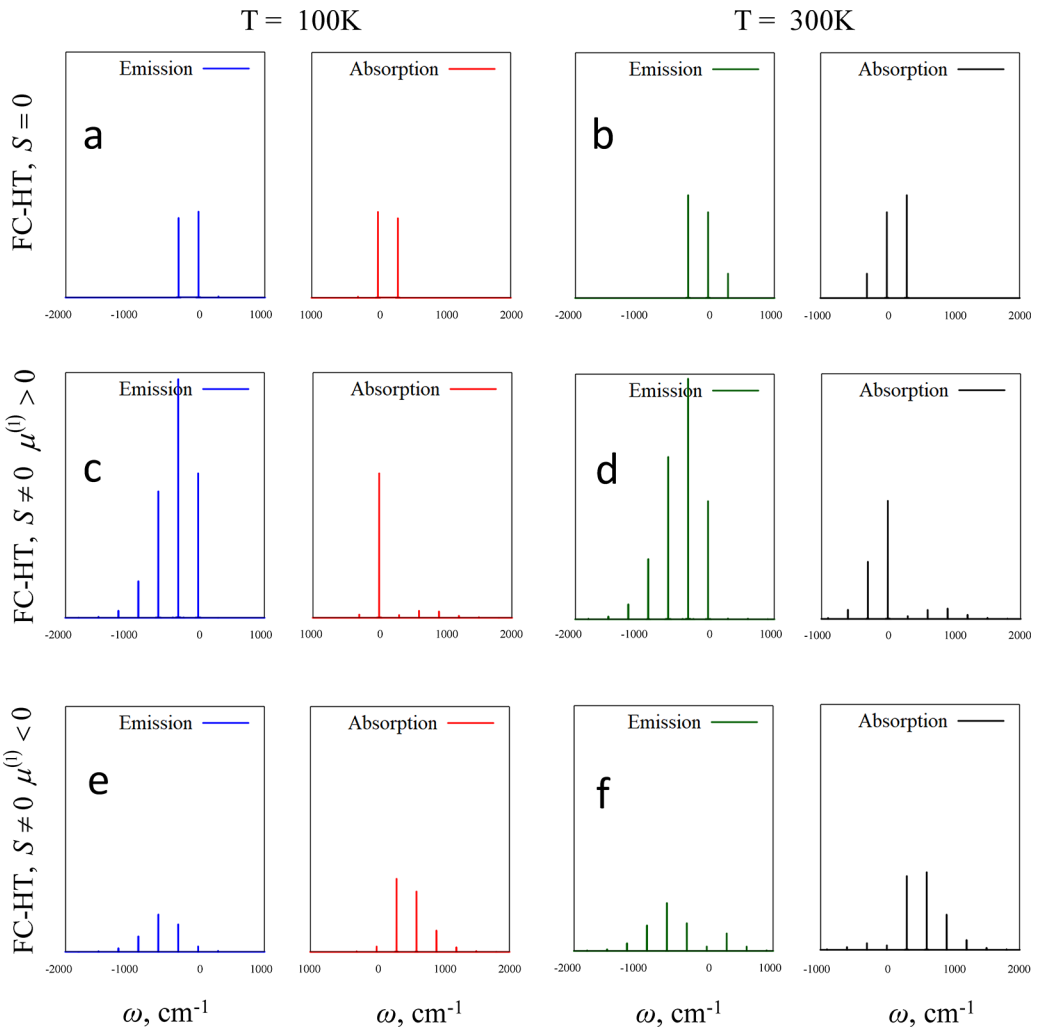


**Figure 4.** FC-HT spectra for $\omega_1$ = 300 cm$^{-1}$. The frequency axes have been shifted by $(\varepsilon_e - \varepsilon_g)/\hbar$. (a, b) Symmetric spectra with $|\mu_1^{(1)}|\Delta s/\mu^{(0)}$ = 0.05, $S$ = 0. (c, d) Spectra for$\mu^{(0)}$ = 1, $\mu_1^{(1)}\Delta s/\mu^{(0)}$ = 0.05, $S_1$ = 0.5 where dipole-expansion and interference effects cooperate. (e, f) $\mu_1^{(1)}\Delta s/\mu^{(0)}$ = −0.05, $S$ = 0.5 when the two effects are in competition. The vertical axis range in Figure 4 panels has been doubled compared to Figure 3, so that the higher peak intensities could be accommodated. Left: $T$ = 100 K. Right: $T$ = 300 K.

identical frequencies and dipole moments, but different Huang−Rhys factors can exhibit opposite trends in the absorption and emission intensities.

## 4. ABSORPTION−EMISSION ASYMMETRY FOR DISCRETE MODES

In this section, we present absorption and emission spectra at two temperatures (100 and 300 K) for various combinations of vibrational parameters. Apart from the characteristic vibrational frequencies and Huang−Rhys factors that determine the respective displacements between the potential minima, the vibrational modes can be classified into four categories:

(i) Purely FC-active ($\mu^{(0)} \neq 0$, $\mu_k^{(1)} = 0$),
(ii) Purely HT-active ($\mu^{(0)} = 0$, $\mu_k^{(1)} \neq 0$),
(iii) FC-HT-active with components that satisfy $\tilde{\mu}^{(0)} = \mu^{(0)} + \frac{1}{2}\sum_k \mu_k^{(1)}\Delta q_{ge}^{eq} = 0$, and
(iv) FC-HT-active ($\mu^{(0)} \neq 0$, $\mu_k^{(1)} \neq 0$) in the general case $\tilde{\mu}^{(0)} \neq 0$.

We show results for discrete modes with frequencies equal to 300 and 500 cm$^{-1}$ for Huang−Rhys factors in the range of 0−0.8. For nonzero values of $\mu^{(0)}$, we quantify the dipole moment parameters through the dimensionless ratio $\mu_k^{(1)}\Delta s/\mu^{(0)}$. If either $\mu^{(0)}$ = 0 or $\mu_k^{(1)}$ = 0, the dipole moment value simply rescales the line intensity, so we do not specify it.

We begin with the spectral behaviors arising from a single vibrational mode and the manifestations of mirror symmetry breaking between absorption and emission. We then focus on the signatures of combination bands for pairs of vibrational modes of different dipole characters and the homogeneous broadening from hundreds of weakly coupled bath modes at finite temperatures.

**4.1. Single-Mode Spectra and Loss of Mirror-Image Symmetry.** Figure 3a,b shows the spectra for a single vibrational mode with frequency $\omega_1$ under the Franck−Condon approximation $\mu_1^{(1)}$ = 0. As expected, the absorption and emission spectra exhibit progressions arising from vertical transitions between vibrational levels in the ground and excited electronic states encoded in the $R^{FC}$ term. The frequencies for the observed transitions are $\omega_1 = (\varepsilon_e - \varepsilon_g)/\hbar \pm m_1\omega_1$, where $m_1$ is a non-negative integer. The frequency axes of the spectra in Figure 3 and all subsequent figures have been shifted by the electronic frequency $(\varepsilon_e - \varepsilon_g)/\hbar$, such that the 0−0 transition peak lies at 0. The relative intensities of the vibronic progressions depend on the Franck−Condon overlaps between


https://doi.org/10.1021/acs.jpcb.2c00846
J. Phys. Chem. B 2022, 126, 2899−2911

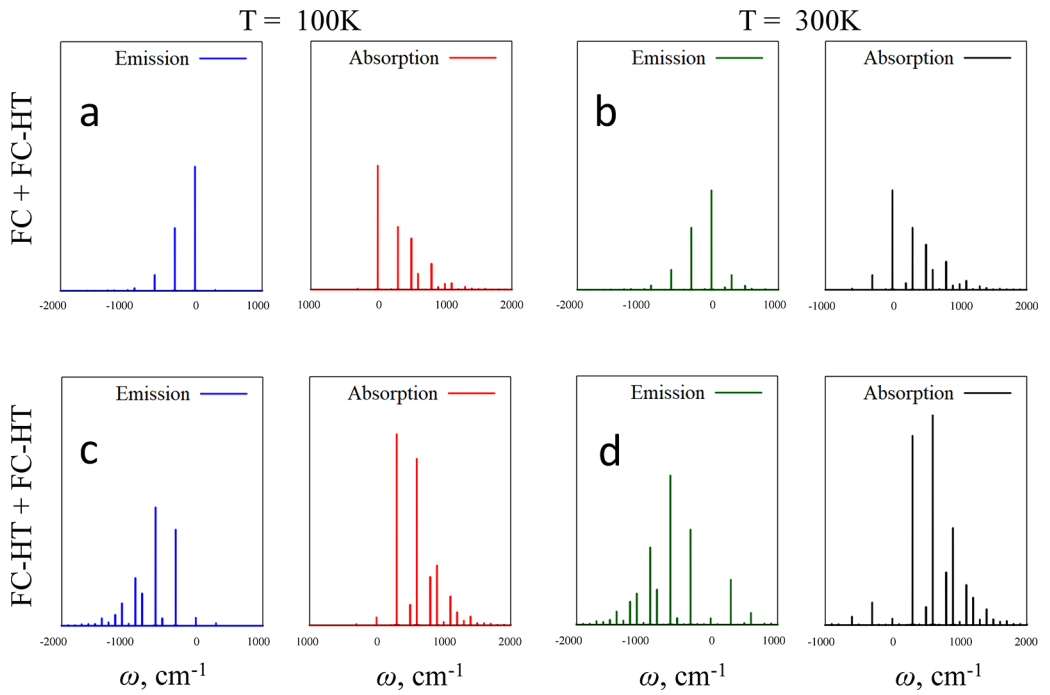


**Figure 5.** Absorption and emission spectra for a molecule with a two vibrational modes of frequencies $\omega_1$ = 300 cm$^{-1}$ and $\omega_2$ = 500 cm$^{-1}$. The frequency axes have been shifted by $(\varepsilon_e - \varepsilon_g)/\hbar$. (a, b) One FC mode with $\mu_1^{(1)}\Delta s/\mu^{(0)} = 0$, $S_1 = 0.5$ and one FC-HT mode with $\mu_1^{(1)}\Delta s/\mu^{(0)} = -0.02$, $S_2 = 0.1$. (c, d) Two FC-HT modes: $\mu_1^{(1)}\Delta s/\mu^{(0)} = -0.05$, $S_1 = 0.5$ and $\mu_2^{(1)}\Delta s/\mu^{(0)} = 0.05$, $S_2 = 0.1$. Left: $T$ = 100 K. Right: $T$ = 300 K.

the relevant states, which have a nonmonotonic dependence on the quantum numbers and the potential surface separation (i.e., the electron-vibration coupling or the Huang−Rhys factor). At low temperature, most of the peak intensities correspond to transitions from the ground vibrational level of the ground electronic state. As the temperature is increased, new transitions emerge from vibrationally excited states, leading to a rescaling of peak intensities. We note the perfect mirror symmetry between absorption and emission spectra in the pure FC case.

Next, in Figure 3c,d, we focus on spectra that arise exclusively from HT coupling, i.e., $\mu^{(0)} = 0$ in eq 2.10, such that the only contributing term is $R^{HT}$. As discussed in the previous section, the asymmetry that results from linearization of the dipole moment with respect to one of the two potential minima results in FC-HT interference and the loss of mirror-image symmetry between absorption and emission spectra. With the exception of the $n-n$ transition peak (at $\omega = 0$), absorption and emission spectral lines are seen to have different intensities. Figure 3e,f shows that the absorption−emission symmetry is restored in the FC-HT spectra obtained with $\tilde{\mu}^{(0)} = 0$, i.e., in a pure HT transition originating from a dipole moment that is linear about the midpoint between the two potential minima. We also note that because of the symmetric placement of the point of expansion and the absence of the FC term, the $n-n$ transition peak vanishes in this limit.

Figure 4a,b shows the spectra with both FC and HT terms in the dipole-expansion (with generic parameters that lead to $\tilde{\mu}^{(0)} \neq 0$) for the special case $S_1 = 0$. This limit is relevant for vibrations that are not FC-coupled (or are very weakly coupled) to the electronic states but possess sizable HT contributions. Since the ground and excited surfaces are undisplaced in this case, the $n-n$ peak is of a purely FC origin, and the only allowed vibrational transitions ($n \rightarrow n\pm1$) arise entirely from the linear term in the normal mode coordinate (i.e., are purely HT). Thus, three peaks are observed with no interference (i.e., $R^{FC-HT}$ vanishes when the Huang−Rhys factor is equal to zero). The $R^{HT}$ term is perfectly symmetric in this case because the two potential surfaces lie on top of each other; thus, the absorption and emission intensities are equal. As expected, the relative intensity of the $n+1 \rightarrow n$ peak is increased with temperature due to the population of the excited vibrational levels.

When $S_1 \neq 0$ (Figure 4c−f), all three terms in the correlation function, including the $R^{FC-HT}$ term, contribute to each peak, and mirror symmetry is broken for all $n-n'$ transitions. As is evident from eqs 3.17 and 3.18, the enhancement of the absorption or emission intensities depends on the sign of the $\mu_1^{(1)}$. Figure 4c,d shows spectra with $\mu^{(0)} > 0$, $\mu_1^{(1)} > 0$. In agreement with the conclusions of the previous section, it is seen that the intensities of the peaks that lie on the right of the 0−0 absorption line are weaker than those on the left of the 0−0 emission line. The converse holds for lines on the other sides of the 0−0 lines. The opposite situation is illustrated in Figure 4e,f, where $\mu^{(0)} > 0$, $\mu_1^{(1)} < 0$. In this case, absorption intensities are larger on the right side of the spectrum compared to their emission counterparts. Further, the opposite signs of these two parameters lead to significant decrease in the value of $\tilde{\mu}^{(0)}$ compared to the previous case, which causes the absorption−emission asymmetry to be less prominent.

**4.2. Combination Peaks.** In a molecule with many coupled vibrations, electronic transitions are accompanied by the simultaneous excitation/de-excitation of multiple modes, leading to combination peaks that lie at the cumulative transition frequencies $\omega = (\varepsilon_e - \varepsilon_g)/\hbar \pm m_1\omega_1 \pm m_2\omega_2 \pm m_3\omega_3 \pm \cdots$ where $m_1$, $m_2$, $m_3\cdots$ are non-negative integers. Figure 5 shows spectra for pairs of vibrations. It is easily seen that combination peaks exhibit asymmetric intensities only


https://doi.org/10.1021/acs.jpcb.2c00846
J. Phys. Chem. B 2022, 126, 2899−2911

when at least one of the participating transitions is asymmetric. For example, in Figure 5a,b, the vibronic peaks associated with the selective excitation or de-excitation of the FC mode are perfectly symmetric, whereas the vibronic progressions of the FC-HT mode and the combination peaks involving transitions of both modes are asymmetric. Similar assignments of peaks can be made in Figure 5c,d for a pair of FC-HT-active modes, where all $n-n'$ transitions exhibit dipole-expansion and interference asymmetries. Depending on the relative signs of the HT couplings, interferences (in absorption for example) are either (i) both constructive/both destructive, as in Figure 5c,d or (ii) constructive for one mode and destructive for the other (this example is shown in Section 5). Both cases are usually encountered in multimode spectra.

## 5. HOMOGENEOUS BROADENING, PEAK POSITION ASYMMETRY, AND TEMPERATURE DEPENDENCE

In this section, we show the changes to the spectra due to the presence of an FC-active dissipative bath, which mimics the effect of a solvent or matrix environment. Solvent spectral densities typically comprise a dense manifold of modes at relatively low frequencies that capture the translational, rotational, and slow vibrational motions of the nuclei. Spectra in solution thus comprise a host of transitions between a large number of accessible levels, making the underlying fine structure impossible to resolve.

We choose a harmonic dissipative bath described by the well-known Ohmic spectral density[31]

$$J(\omega) = \frac{2}{\Delta s^2}\pi\hbar\xi\ \omega e^{-\omega/\omega_c} \tag{5.1}$$

which peaks at $\omega_c$ = 300 cm$^{-1}$, and the dimensionless parameter $\xi = \frac{1}{3}$ characterizes the strength of coupling to the electronic states. The system-bath coupling strength is often quantified in terms of the reorganization energy, which with the present parameters is $\lambda$ = 200 cm$^{-1}$. While computing response functions, we discretize the Ohmic bath into 200 normal modes using a logarithmic scheme,[32,33] which amounts to a uniform partitioning of the reorganization energy. The bath modes are assumed to be purely of FC character.

The dense manifold of transitions from the bath lead to a spectral envelope over a broad frequency range. The absorption and emission spectra that result from coupling the two electronic states to only the bath are shown by gray lines in Figure 6a. Note that the reorganization energy of the bath is not necessarily reflected in the Stokes shift between the absorption and emission peaks.[34] Moreover, when the dissipative bath (or the solvent) is included alongside other discrete vibrations with relatively stronger FC or HT couplings (e.g., intramolecular normal modes), a multitude of peaks that arise from the combination of bath and discrete modes are observed. The resulting spectra are shown in Figure 6 for a single discrete mode of FC or combined FC-HT activity. It is seen that the bath gives rise to broadening around the previously observed sharp peaks, which now form spectral bands. Note that the observed broadening is entirely homogeneous and arises from the dynamical effects of explicit modes with incommensurate frequencies and coupling strengths. Although the pure FC bath spectra preserve mirror symmetry, coupling of an FC-HT-active mode to a bath (Figure 6b,c) results in asymmetry that arguably is even more pronounced in comparison to the spectra of the same mode

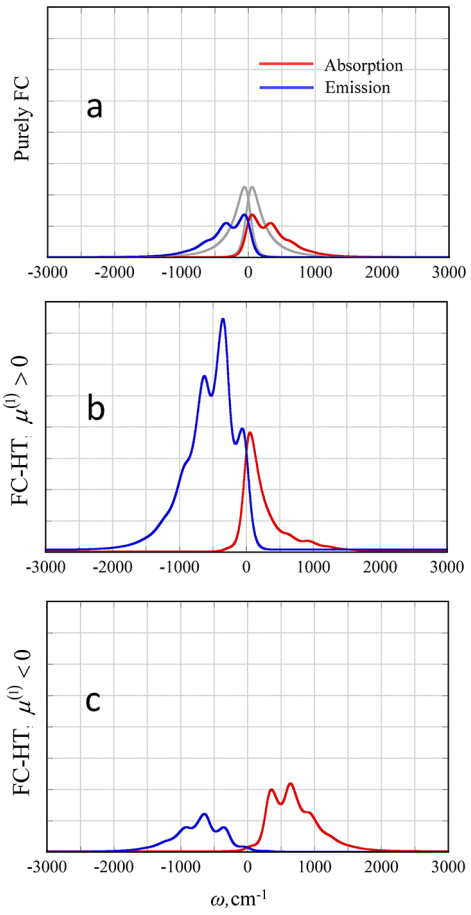


**Figure 6.** Homogeneous broadening effects (at $T$ = 100 K) of a dissipative bath on single-mode spectra: $\omega_1$ = 300 cm$^{-1}$ and $S_1$ = 0.5. In all cases, the electronic states are coupled to an Ohmic bath having $\omega_c$ = 300 cm$^{-1}$ and $\xi$ = 0.33. (a) FC mode: $\mu_1^{(1)}\Delta s/\mu^{(0)}$ = 0. The spectra obtained for the bath alone are shown with gray lines. FC-HT spectra with (b) $\mu_1^{(1)}\Delta s/\mu^{(0)}$ = 0.05 and (c) $\mu_1^{(1)}\Delta s/\mu^{(0)}$ = − 0.05. The frequency axes have been shifted by $(\varepsilon_e - \varepsilon_g)/\hbar$.

without the bath (Figure 4c,e). This is so because the asymmetric HT component of the discrete mode forms combination bands with the FC-active bath, leading to a nontrivial structural modulation of the lineshape.

We previously noted in Figure 5c,d how the relative magnitudes and signs of the dipole derivatives modulate absorption−emission asymmetry when two FC-HT-active modes are coupled together. Figure 7 shows the effect of the bath on such spectral trends. We now consider modes with the same frequencies ($\omega_1$ = 300 cm$^{-1}$ and $\omega_2$ = 500 cm$^{-1}$) but with smaller FC coupling, such that each mode by itself results primarily in one or two prominent vibronic peaks ($n \rightarrow n$ and $n \rightarrow n \pm 1$) and single-mode effects of symmetry breaking are less prominent. As discussed earlier, when the HT couplings of the two vibrations are of the same sign (Figure 7a), the directions of absorption−emission asymmetry are aligned, resulting in large asymmetry effects overall. As a result, the $n \rightarrow n$+1 peaks for both modes are visible over the spectral envelope in emission spectra, whereas in absorption, destructive interference reduces the intensities of both transitions leaving behind only the $n-n$ peak and a minor shoulder at larger frequencies.

When the HT couplings differ in sign, the directions of asymmetry are opposite and the intensities of transitions can



https://doi.org/10.1021/acs.jpcb.2c00846
J. Phys. Chem. B 2022, 126, 2899−2911

be more commensurate. However, if the two mode frequencies differ, the opposite asymmetries appear at different frequencies, creating peaks of opposing intensities. As seen in Figure 7b, the contrasting nature of interferences for the two vibrational modes causes the $n \rightarrow n+1$ transition of one mode (with $\omega_2$ = 500 cm$^{-1}$) to be only visible in the absorption spectrum, while the other ($\omega_1$ = 300 cm$^{-1}$) is only visible in fluorescence. The central peaks near $\omega = 0$ consist of $n-n$ transitions for the discrete modes and vibrational progressions of bath modes. Similar asymmetric shifts are very prominent in several of the panels shown in Figures 6−8. In Figure 7a, the strongest peak

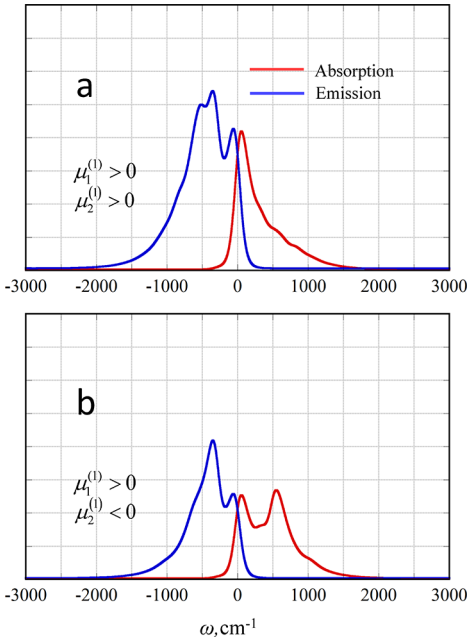


**Figure 7.** Spectra for two relatively weakly coupled FC-HT modes in the presence of the bath, $\omega_1$ = 300 cm$^{-1}$, $S_1$ = 0.1 and $\omega_2$ = 500 cm$^{-1}$, $S_2$ = 0.05: (a) where both HT couplings are positive, $\mu_1^{(1)}\Delta s/\mu^{(0)}$ = 0.05 and $\mu_2^{(1)}\Delta s/\mu^{(0)}$ = 0.05, and (b) where the HT couplings are of different signs, $\mu_1^{(1)}\Delta s/\mu^{(0)}$ = 0.05 and $\mu_2^{(1)}\Delta s/\mu^{(0)}$ = 0.05. Bath parameters are identical to those in Figure 5, and both panels show spectra at $T$ = 100 K. The frequency axes have been shifted by $(\varepsilon_e - \varepsilon_g)/\hbar$.

in the emission spectrum is around ∼350 cm$^{-1}$ (from mode $\omega_1$), while the highest peak in absorption is that of the $n-n$ transition (shifted by the bath to ∼60 cm$^{-1}$). The asymmetric shift effect is even more clearly seen in Figure 9a (discussed later), which shows spectra at a higher temperature that consist of a single broad band. While the maximum of the absorption spectrum remains at ∼60 cm$^{-1}$, the fluorescence peak now lies around 480 cm$^{-1}$. Asymmetry in the peaks of absorption and emission spectra may be erroneously assigned to the difference in the vibrational frequencies in the ground and excited potential surfaces.

As explained in Section 3, the absorption−emission asymmetry disappears (and the spectra of FC-HT-active modes simplify) when the Huang−Rhys factor is equal to zero and (if $\mu^{(0)}\mu^{(1)} < 0$) for another critical value $S_c$. In the latter case, the spectral asymmetry switches signs as the mode Huang−Rhys factor is increased. Figure 8 illustrates this effect. It is seen that for the smallest value $S_1$ = 0.1, the absorption intensity is larger, while for the larger value $S_1$ = 0.8, the fluorescence becomes stronger. With the chosen parameters,

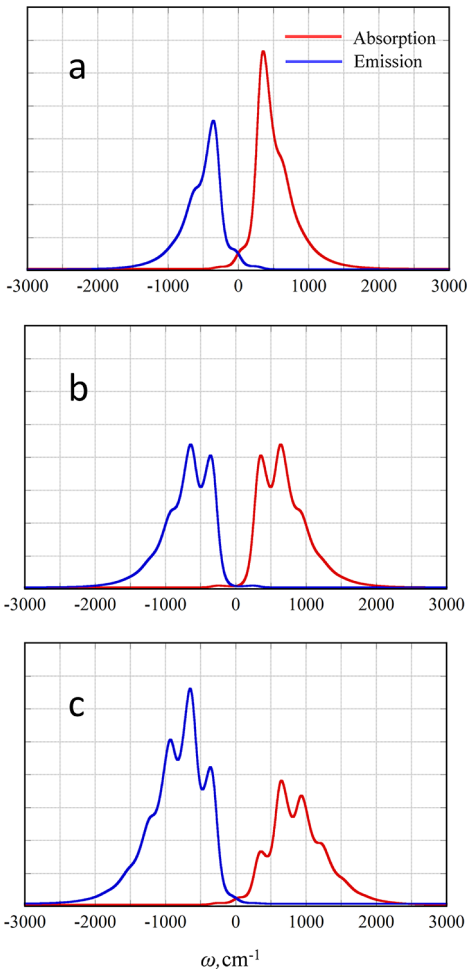


**Figure 8.** Inversion of absorption−emission asymmetry through variation of the Huang−Rhys factor for a discrete mode with $\omega$ = 300 cm$^{-1}$ at $T$ = 100 K with $\mu_1^{(1)}\Delta s/\mu^{(0)}$ = − 0.0833 coupled to a dissipative bath with the parameters given in the main text. (a) $S_1$ = 0.1. (b) $S_1$ = 0.39366 such that $\tilde{\mu}^{(0)} = 0$. (c) $S_1$ = 0.8. The frequency axes have been shifted by $(\varepsilon_e - \varepsilon_g)/\hbar$.

the spectra exhibit perfect mirror symmetry for the critical value $S_1$ = 0.39366.

Last, we investigate in Figure 9 the effect of temperature on the spectra in the presence of a bath. With increase in the available thermal energy, vibronic peaks and combination bands that involve transitions from higher vibrational states become accessible. The emergence of a larger number of higher vibronic transitions and combination bands leads to broadening and modulation of peaks irrespective of their dipole characters. In Figure 9a, we show the changes in the spectra obtained with the parameters used in Figure 6b upon increasing the temperature from 100 to 300 K. At $T$ = 100 K, most visible transitions are of the $m < n$ type, leading to a dominant emission spectrum. However, as the temperature is increased, strong $m > n$ transitions emerge in the $\omega < 0$ region (marked by a magenta arrow) of the absorption spectrum as excited vibrational states become thermally accessible. Such transitions are not visible in the emission spectrum, leaving the analogous $\omega > 0$ region empty. This effect more than compensates for the usual blueshift of the absorption spectra, leading to the impression of an anomalous redshift. The trends are reversed with $\mu_1^{(1)} > 0$ (Figure 9b) now generating new intensity (magenta arrow) in the emission spectrum.



https://doi.org/10.1021/acs.jpcb.2c00846
J. Phys. Chem. B 2022, 126, 2899−2911

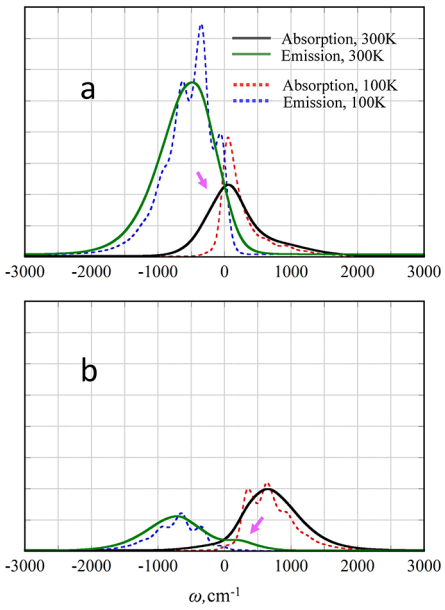


**Figure 9.** Temperature dependence of bath spectra. (a, b) Spectra at $T = 300$ K for a single FC-HT mode, $\omega_1 = 300$ cm$^{-1}$ and $S_1 = 0.5$ with different directions of asymmetry, (a) $\mu_1^{(1)}\Delta s/\mu^{(0)} = 0.05$ and (b) $\mu_1^{(1)}\Delta s/\mu^{(0)} = -0.05$. The analogous low temperature results previously shown in Figure 6b,c respectively, have been replotted with dashes to aid comparison. Bath parameters are identical to Figures 5 and 6. The frequency axes have been shifted by $(\varepsilon_e - \varepsilon_g)/\hbar$.

The spectrum of a chromophore with multiple FC-HT-active modes may comprise combinations of the aforementioned effects. Such multimode signatures create nontrivial temperature-dependent modulations in spectra, some of which have been emulated in this paper within the realms of a simple model.

## 6. CONCLUDING REMARKS

Molecules that display significant deviations from simple Franck–Condon transitions give rise to interesting and sometimes unexpected spectral characteristics. In this paper, we presented a comprehensive study of FC-HT signatures in the linear spectra of model molecular systems within the normal mode approximation, where the two relevant electronic states are described by multidimensional harmonic potential surfaces. We have shown analytically that the asymmetry induced by the interference of FC and HT components has opposite signs for all transitions in equivalent sides of the 0–0 line in the absorption and emission spectra (e.g., the blue side in absorption and red side in emission, or vice versa) and that the trend is reversed for all transitions on the other of the 0–0 line.

For each vibrational mode, the absorption–emission asymmetry depends on the dipole moment parameters as well as the mode frequency and Huang–Rhys factor. We have obtained a simple relation for the asymmetry and shown that it vanishes not only in simple limits corresponding to undisplaced potential surfaces or to particular relations of the dipole moment parameters but also for nontrivial parameter combinations. As a result, a crossover is observed from the spectra where fluorescence intensities are more prominent to the spectra where absorption dominates. In molecular systems comprising many vibrational modes, similar or opposing trends in line intensities can give rise to interesting spectral features. As the thermal population of the vibrational levels modulates peak intensities in the blue and red sides of the 0–0 line, the HT-induced asymmetry can impact the temperature dependence of molecular spectra in nontrivial ways.

Our analytical results were illustrated by numerically exact calculations in models of one or two discrete vibrational modes using parameters typical of common molecular systems as well as in the presence of an FC-active dissipative bath that mimics a condensed-phase environment and accounts for homogeneous broadening. The computed spectra illustrate the nontrivial FC-HT interference that causes the breakdown of absorption–emission symmetry, its recovery through accidental symmetries, and its inversion by minor changes in coupling strengths. The inclusion of a dissipative bath gives rise to diverse and very rich spectral patterns, which arise from the combination bands of HT-active molecular vibrations and a large number of FC-active bath modes. In addition to spectral broadening, we observed large asymmetric peak shifts, which produce the illusion of unequal vibrational frequencies in the two potential surfaces. Finally, thermal effects were seen to unequally impact the asymmetry across spectral regions, leading to intriguing trends in the spectra. We expect these interesting trends to be largely observable in the condensed-phase spectra of HT-active molecular systems.

## APPENDIX A

Here, we provide an outline of the procedure for computing linear absorption and emission spectra under the Herzberg–Teller approximation. For a transition from electronic state $|a\rangle$ to state $|b\rangle$, the response function has the form

$$R(t) = Z^{-1}\mathrm{Tr}(\hat{\mu}e^{-i\hat{H}_b t/\hbar}\hat{\mu}\, e^{-\beta\hat{H}_a}e^{i\hat{H}_a t/\hbar}) \tag{6.1}$$

For general Hamiltonians, this expression may be evaluated in the semiclassical limit as a special case of the quantum-classical path integral[26−28] (QCPI) expression. For the present purpose where the vibrational Hamiltonians are quadratic functions, the QCPI procedure is exact. Further, with the normal mode form of the two potential surfaces, each component of the response function factorizes into single-mode correlation functions. Shifting the coordinates, the vibrational Hamiltonians can be written as

$$\hat{H}_a = \sum_k \hat{h}_{a,k} = \sum_k \frac{\hat{p}_k^2}{2m} + \frac{1}{2}m\omega_k^2\hat{q}_k^2$$

$$\hat{H}_b = \sum_k \hat{h}_{b,k} = \sum_k \frac{\hat{p}_k^2}{2m} + \frac{1}{2}m\omega_k^2(\hat{q}_k - q_{b,k}^{\mathrm{eq}})^2 \tag{6.2}$$

with $q_{b,k}^{\mathrm{eq}} = c_k s_b/m\omega_k^2$. Further, within the FC-HT approximation, the dipole can be expressed in the form

$$\mu(\mathbf{q}) \simeq \mu_{\mathrm{ref}}^{(0)} + \sum_k \mu_k^{(1)}(\hat{q}_k - q_{\mathrm{ref},k}^{\mathrm{eq}}) \tag{6.3}$$

where $\{q_{\mathrm{ref},k}^{\mathrm{eq}}\}$ are the coordinates of the point about which the dipole moment function is expanded in the present coordinate system. The terms entering the response function can be written as

$$R^{\mathrm{FC}}(t) = e^{-i(\varepsilon_b-\varepsilon_a)t/\hbar}(\mu_{\mathrm{ref}}^{(0)})^2\prod_k F_k \tag{6.4}$$



https://doi.org/10.1021/acs.jpcb.2c00846
J. Phys. Chem. B 2022, 126, 2899−2911

$$R^{\mathrm{HT}}(t) = e^{-i(\varepsilon_b-\varepsilon_a)t/\hbar}\sum_k (\mu_k^{(1)})^2(F_k^{\langle qq\rangle} - 2q_{\mathrm{ref},k}^{\mathrm{eq}}F_k^{\langle q\rangle} + (q_{\mathrm{ref},k}^{\mathrm{eq}})^2F_k)\prod_{j\neq k}F_j + e^{-i(\varepsilon_b-\varepsilon_a)t/\hbar}\sum_k\sum_{k'\neq k}\hat{\mu}_k^{(1)}\hat{\mu}_{k'}^{(1)}(F_k^{\langle q\rangle}F_{k'}^{\langle q\rangle} - q_{\mathrm{ref},k}^{\mathrm{eq}}F_kF_{k'}^{\langle q\rangle} - q_{\mathrm{ref},k}^{\mathrm{eq}}F_kF_k^{\langle q\rangle} + q_{\mathrm{ref},k}^{\mathrm{eq}}q_{\mathrm{ref},k}^{\mathrm{eq}}F_kF_{k'})\prod_{j\neq k,k'}F_j \tag{6.5}$$

$$R^{\mathrm{FC-HT}}(t) = 2e^{-i(\varepsilon_b-\varepsilon_a)t/\hbar}\mu_{\mathrm{ref}}^{\mathrm{vib},(0)}\sum_k \mu_k^{(1)}(F_k^{\langle q\rangle} - q_{\mathrm{ref},k}^{\mathrm{eq}}F_k)\prod_{j\neq k}F_j \tag{6.6}$$

where

$$F_k = Z_k^{-1}\mathrm{Tr}(e^{-i\hat{h}_{b,k}t/\hbar}e^{-\beta\hat{h}_{a,k}}e^{i\hat{h}_{a,k}t/\hbar}) \tag{6.7}$$

is the FC line broadening function,

$$F_k^{\langle q\rangle} = Z_k^{-1}\mathrm{Tr}(\hat{q}_k e^{-i\hat{H}_{b,k}t/\hbar}e^{-\beta\hat{h}_{a,k}}e^{i\hat{H}_{a,k}t/\hbar}) \tag{6.8}$$

is reminiscent of the "average coordinate" of the $k^{\mathrm{th}}$ normal mode, and

$$F_k^{\langle qq\rangle} = Z_k^{-1}\mathrm{Tr}(\hat{q}_k e^{-i\hat{h}_{b,k}t/\hbar}\hat{q}_k e^{-\beta\hat{h}_{a,k}}e^{i\hat{h}_{a,k}t/\hbar}) \tag{6.9}$$

resembles a "position correlation function."

Each of these functions may be written in the QCPI form. Dropping the mode subscript $k$, eqs 6.7 to 6.9 can be obtained from the expression

$$C_{AB} = \int dq_0 \int dp_0\, W_A(q_0, p_0)B(q_t, p_t)e^{i\theta(q_0,p_0)/\hbar} \tag{6.10}$$

where $W_A$ is the Wigner phase space transform of the operator $\hat{A}\, e^{-\beta\hat{h}_{a,k}}/Z_k$, $q_t$, $p_t$ are the phase space coordinates reached by a classical trajectory to be specified below, $\theta$ is the QCPI phase, and the operators $\hat{A}$, $\hat{B}$ are equal to $\hat{q}$ or $\hat{I}$ (the identity). The classical trajectory is subject to the average of the forces supplied by the two Hamiltonians, i.e., $\frac{1}{2}cs_b$. The position reached by the trajectory at the time $t$ is

$$q(t) = q_0\cos\omega t + \frac{p_0}{m\omega}\sin\omega t + \frac{cs_b}{2m\omega^2}(1-\cos\omega t) \tag{6.11}$$

and the classical phase is given by

$$\theta(t) = \frac{cq_0s_b}{\omega}\omega t + \frac{cp_0s_b}{m\omega^2}(1-\cos\omega t) - \frac{c^2s_b^2}{2m\omega^3}\sin\omega t \tag{6.12}$$

The last term arises from the difference of the coordinate-independent term of $q(t)$ and the quadratic "counterterm" in $H_b$ (which encodes the vibrational reorganization energy between the two surfaces). Last, the Wigner functions are

$$W_I(q_0, p_0) = \frac{1}{\pi\hbar}\tanh\left(\frac{1}{2}\beta\hbar\omega\right)e^{-\tanh(\frac{1}{2}\beta\hbar\omega)(\frac{m\omega q_0^2}{\hbar}+\frac{p_0^2}{m\omega\hbar})} \tag{6.13}$$

$$W_q(q_0, p_0) = \left(q_0 - i\frac{p_0}{m\omega}\right)W_I(q_0, p_0) \tag{6.14}$$

The resulting QCPI integrals are Gaussian and may be evaluated analytically to yield closed-form expressions for $F_k$, $F_k^{\langle q\rangle}$, and $F_k^{\langle qq\rangle}$.

## AUTHOR INFORMATION


### Corresponding Author

**Nancy Makri** − *Department of Chemistry, University of Illinois, Urbana, Illinois 61801, United States; Department of Physics and Illinois Quantum Information Science and Technology Center, University of Illinois, Urbana, Illinois 61801, United States;* orcid.org/0000-0002-3310-7328; Email: nmakri@illinois.edu

### Authors

**Sohang Kundu** − *Department of Chemistry, University of Illinois, Urbana, Illinois 61801, United States;* orcid.org/0000-0002-5499-9775

**Partha Pratim Roy** − *Department of Chemistry, University of California, Berkeley, California 94720, United States; Molecular Biophysics and Integrated Bioimaging Division, Lawrence Berkeley National Laboratory, Berkeley, California 94720, United States; Kavli Energy Nanoscience Institute at Berkeley, Berkeley, California 94720, United States;* orcid.org/0000-0003-3202-4333

**Graham R. Fleming** − *Department of Chemistry, University of California, Berkeley, California 94720, United States; Molecular Biophysics and Integrated Bioimaging Division, Lawrence Berkeley National Laboratory, Berkeley, California 94720, United States; Kavli Energy Nanoscience Institute at Berkeley, Berkeley, California 94720, United States;* orcid.org/0000-0003-0847-1838

Complete contact information is available at: https://pubs.acs.org/10.1021/acs.jpcb.2c00846


### Notes

The authors declare no competing financial interest.

## ACKNOWLEDGMENTS

This material is based upon work supported by the National Science Foundation Center for Synthesizing Quantum Coherence under grant no. 1925690.

## REFERENCES


(1) Condon, E. U. Nuclear Motions Associated with Electron Transitions in Diatomic Molecules. *Phys. Rev.* **1928**, *32*, 858−872.

(2) Herzberg, G., *Molecular spectra and molecular structure*. 22nd ed.; D. Van Nostrand: New York, 1950; Vol. *1*.

(3) Zgierski, M. Z. Herzberg-Teller interactions and spectra of dimers: Stable anthracene dimer. *J. Chem. Phys.* **1973**, *59*, 3319−3322.

(4) Craig, D. P.; Small, G. J. Totally Symmetric Vibronic Perturbations and the Phenanthrene 3400-Å Spectrum. *J. Chem. Phys.* **1969**, *50*, 3827−3834.

(5) Kano, H.; Saito, T.; Kobayashi, T. Observation of Herzberg−Teller-type Wave Packet Motion in Porphyrin J-Aggregates Studied by Sub-5-fs Spectroscopy. *J. Phys. Chem. A* **2002**, *106*, 3445−3453.

(6) Kee, H. L.; Bhaumik, J.; Diers, J. R.; Mroz, P.; Hamblin, M. R.; Bocian, D. F.; Lindsey, J. S.; Holten, D. Photophysical characterization of imidazolium-substituted Pd(II), In(III), and Zn(II) porphyrins as photosensitizers for photodynamic therapy. *J. Photochem. Photobiol., A* **2008**, *200*, 346−355.

(7) Ballhausen, C. J.; Hansen, A. E. Electronic Spectra. *Annu. Rev. Phys. Chem.* **1972**, *23*, 15−38.

(8) Azumi, T.; Matsuzaki, K. WHAT DOES THE TERM "VIBRONIC COUPLING" MEAN? *Photochem. Photobiol.* **1977**, *25*, 315−326.

(9) Teller, G. H. a. E. *Z. Physik. Chem. (Leipzig)* **1933**, *B21*, 410.

(10) Struve, W. S., *Fundamentals of molecular spectroscopy*. New York, 1989.




https://doi.org/10.1021/acs.jpcb.2c00846
J. Phys. Chem. B 2022, 126, 2899−2911

(11) Small, G. J. Herzberg−Teller Vibronic Coupling and the Duschinsky Effect. *J. Chem. Phys.* **1971**, *54*, 3300−3306.
(12) Hohlneicher, G.; Wolf, J. Interference between Franck-Condon and Herzberg-Teller Contributions in Naphthalene and Phenanthrene. *Ber. Bunsengesellschaft Phys. Chem.* **1995**, *99*, 366−369.
(13) Macak, P.; Luo, Y.; Ågren, H. Simulations of vibronic profiles in two-photon absorption. *Chem. Phys. Lett.* **2000**, *330*, 447−456.
(14) Santoro, F.; Lami, A.; Improta, R.; Bloino, J.; Barone, V. Effective method for the computation of optical spectra of large molecules at finite temperature including the Duschinsky and Herzberg−Teller effect: The Qx band of porphyrin as a case study. *J. Chem. Phys.* **2008**, *128*, 224311.
(15) Baiardi, A.; Bloino, J.; Barone, V. General Time Dependent Approach to Vibronic Spectroscopy Including Franck−Condon, Herzberg−Teller, and Duschinsky Effects. *J. Chem. Theory Comput.* **2013**, *9*, 4097−4115.
(16) Karaush, N. N.; Valiev, R. R.; Baryshnikov, G. V.; Minaev, B. F.; Ågren, H. DFT simulation of the heteroannelated octatetraenes vibronic spectra with the Franck−Condon and Herzberg−Teller approaches including Duschinsky effect. *Chem. Phys.* **2015**, *459*, 65−71.
(17) Zhang, H.-D.; Qiao, Q.; Xu, R.-X.; Yan, Y. Effects of Herzberg−Teller vibronic coupling on coherent excitation energy transfer. *J. Chem. Phys.* **2016**, *145*, 204109.
(18) Bizimana, L. A.; Carbery, W. P.; Gellen, T. A.; Turner, D. B. Signatures of Herzberg−Teller coupling in three-dimensional electronic spectroscopy. *J. Chem. Phys* **2017**, *146*, No. 084311.
(19) Pan, Y.; Li, L.; Qiu, F.; Wei, Y.; Hua, W.; Tian, G. On the spectral profile change in the Q band absorption spectra of metalloporphyrins (Mg, Zn, and Pd): A first-principles study. *J. Chem. Phys.* **2019**, *150*, 164308.
(20) Begušić, T.; Vaníček, J. On-the-fly ab initio semiclassical evaluation of vibronic spectra at finite temperature. *J. Chem. Phys.* **2020**, *153*, No. 024105.
(21) Arsenault, E. A.; Schile, A. J.; Limmer, D. T.; Fleming, G. R. Vibronic coupling in energy transfer dynamics and two-dimensional electronic−vibrational spectra. *J. Chem. Phys.* **2021**, *155*, No. 054201.
(22) Duschinsky, F. *Acta Physicochim. URSS* **1937**, *7*, 551.
(23) Heller, E. J. Quantum corrections to classical photodissociation models. *J. Chem. Phys.* **1978**, *68*, 2066−2075.
(24) Mukamel, S., *Principles of nonlinear optical spectroscopy*. Oxford University Press: New York, 1995.
(25) Heller, E. J. The semiclassical way to molecular spectroscopy. *Acct. Chem. Res.* **1981**, *14*, 368−375.
(26) Lambert, R.; Makri, N. Quantum-classical path integral: Classical memory and weak quantum nonlocality. *J. Chem. Phys.* **2012**, *137*, 22A552.
(27) Lambert, R.; Makri, N. Quantum-classical path integral: Numerical formulation. *J. Chem. Phys.* **2012**, *137*, 22A553.
(28) Makri, N. Quantum-classical path integral: A rigorous approach to condensed phase dynamics. *Int. J. Quantum Chem.* **2015**, *115*, 1209−1214.
(29) Feynman, R. P. Space-time approach to non-relativistic quantum mechanics. *Rev. Mod. Phys.* **1948**, *20*, 367−387.
(30) Feynman, R. P.; Hibbs, A. R., *Quantum Mechanics and Path Integrals*. McGraw-Hill: New York, 1965.
(31) Leggett, A. J.; Chakravarty, S.; Dorsey, A. T.; Fisher, M. P. A.; Garg, A.; Zwerger, W. Dynamics of the dissipative two-state system. *Rev. Mod. Phys.* **1987**, *59*, 1−85.
(32) Makri, N. The linear response approximation and its lowest order corrections: an influence functional approach. *J. Phys. Chem. B* **1999**, *103*, 2823−2829.
(33) Walters, P. L.; Allen, T. C.; Makri, N. Direct determination of harmonic bath parameters from molecular dynamics simulations. *J. Comput. Chem.* **2017**, *38*, 110−115.
(34) de Jong, M.; Seijo, L.; Meijerink, A.; Rabouw, F. T. Resolving the ambiguity in the relation between Stokes shift and Huang−Rhys parameter. *Phys. Chem. Chem. Phys.* **2015**, *17*, 16959−16969.


https://doi.org/10.1021/acs.jpcb.2c00846
*J. Phys. Chem. B* 2022, 126, 2899−2911